2007-01-1405

Internal Flow and Cavitation in a Multi-hole Injector for Gasoline Direct-Injection Engines

J. M. Nouri, N. Mitroglou, Y. Yan and C. Arcoumanis
The City University, London, UK

ABSTRACT

A transparent enlarged model of a six-hole injector used in the development of emerging gasoline direct-injection engines was manufactured with full optical access. The working fluid was water circulating through the injector nozzle under steady-state flow conditions at different flow rates, pressures and needle positions. Simultaneous matching of the Reynolds and cavitation numbers has allowed direct comparison between the cavitation regimes present in real-size and enlarged nozzles. The experimental results from the model injector, as part of a research programme into second-generation direct-injection spark-ignition engines, are presented and discussed. The main objective of this investigation was to characterise the cavitation process in the sac volume and nozzle holes under different operating conditions. This has been achieved by visualizing the nozzle cavitation structures in two planes simultaneously using two synchronised high-speed cameras.

Imaging of the flow inside the injector nozzle identified the formation of three different types of cavitation as a function of the cavitation number, C_N. The first is needle cavitation, formed randomly at low C_N (0.5-0.7) in the vicinity of the needle, which penetrates into the opposite hole when it is fully developed. The second is the well known geometric cavitation originating at the entrance of the nozzle hole due to the local pressure drop induced by the nozzle inlet hole geometry with its onset at around C_N=0.75. Finally, and at the same time as the onset of geometric cavitation, string type cavitation can be formed inside the nozzle sac and hole volume having a strong swirl component as a result of the large vortical flow structures present there; these become stronger with increasing C_N. Its link with geometric cavitation creates a very complex two-phase flow structure in the nozzle holes which seems to be responsible for hole-to-hole and cycle-to-cycle spray variations.

Keywords: Multi-hole injectors, gasoline direct-injection engines, nozzle cavitation

INTRODUCTION

Direct-injection spark-ignition (DISI) gasoline engines have received considerable attention over the last few years due to their promise to improve fuel efficiency and reduce exhaust emissions. These benefits have attracted even more the attention of the automotive industry due to the worldwide concern over global warming and the need to meet the stringent emission targets introduced for HC and CO_2 by EC and ACEA, such as the reduction in CO_2 emissions for new cars to 120g/km by 2012 [1]. To achieve these goals, excellent control of stratified charge operation during part load remains the key to the success of DISI technology; this is more pronounced with the second generation direct-injection systems where the combustion chamber design has adopted the close-spacing spray-guided concept [1,2]. Spray-guided systems employ pintle- and multi-hole-type injectors where the injection process, rather than the charge movement, controls the stability of the combustible mixture at the spark plug at the time of ignition. The multi-hole injector seems to offer in addition the highest possible flexibility in adapting the spray pattern to the position of the spark-plug in the combustion chamber in such a way that consistent ignition is guaranteed.

Different ignition or combustion strategies can be achieved by this type of injector by varying the spray angle and the nozzle hole geometry. In order to make efficient use of the offered flexibility and keep the development costs down, the influence of these parameters on the spray shape and the fuel atomization process have to be fully understood. With multi-hole injectors, it is expected that nozzle cavitation enhances jet turbulence, which in turn promotes fuel atomization [3, 4]. On the other hand, cavitation may be associated with hole-to-hole and cycle-to-cycle spray variations although evidence of this is rather limited [5]. The latter is an undesirable feature that can impair spray stability, which is vitally important for the success of the spray-guided concept. Thus detailed knowledge of the internal flow and cavitation characteristics inside multi-hole injectors becomes a prerequisite for the refinement of DISI engines, and this forms the basis of the present investigation.

During the last two decades, the focus of research in quantifying nozzle flow and spray characteristics was on diesel injectors [3-12] using both experimental and CFD techniques capable of visualizing, measuring and calculating the internal flow characteristics of injectors and, in particular, describing the cavitation process which is associated with the local pressure distribution inside the sac volume and adjacent holes. Different types of cavitation have been identified: (i) geometrically induced cavitation which occurs in flow areas with sharp corners such as at the entrance into the nozzle holes, (ii) ‘string’ or ‘vortex’ type cavitation [3, 9, 12] which is the main source of instability in the sprays exiting the

nozzle holes and (iii) 'needle' cavitation [13] which initiates in the vicinity of the needle and extends to the opposite nozzle hole when it is fully developed. Although these forms of cavitation have been identified and investigated in diesel multi-hole nozzles, there is very little evidence of their existence in gasoline injectors of similar design.

Most of the previous investigations on gasoline injection systems have focused on the first generation injectors which were of the swirl atomizer type. Recent research on second generation multi-hole injectors is addressing the impact of differences in the chemical and physical properties of gasoline and diesel fuels and in the operating conditions in the nozzle flow and emerging sprays. Early work [14] on swirl-pressure atomizers visualized the formation of liquid film and measured its thickness inside a small transparent nozzle with a hole of the same size as the real injector for injection pressures up to 70 bar. A simpler transparent channel was used in [15] and the results showed that for gasoline fuel cavitation occurs much sooner than that for diesel. A large scale transparent model of a slit injector was developed in [16]; the flow characteristics in the sac volume were identified and the direct link between the size of the vortices in the hole and the fuel spray pattern was confirmed. **B**y optimizing the design of the injector, the vortex size in the hole was reduced and the stratified mode of engine operation significantly improved.

The recent investigation [2] in a transparent model of a real size single-hole VCO type nozzle for gasoline direct-injection engines has focused on the characterization of the in-nozzle flow and cavitation characteristics. The influence of different nozzle hole parameters on the in-nozzle flow characteristics as well as the link between cavitation and spray break-up were shown for injection pressures up to 40 bar and back pressures up to 16 bar. The authors in [2] have identified three types of cavitation namely the bubble, film and string cavitation and showed that nozzle hole cavitation can only influence the primary spray break-up in the vicinity of the nozzle hole exit. They also showed that needle lift, radius of curvature of the nozzle hole inlet and nozzle hole orientation do exert a significant influence on the onset and development of cavitation. For a multi-hole injector, however, the cavitation characteristics may be significantly different than those of [2] due to differences in the local flow, including the large scale vortical structures and turbulence in the sac volume.

The present experimental investigation is concerned with the internal flow and cavitation characteristics in an enlarged 3-D transparent model of a six-hole mini-sac nozzle for gasoline direct-injection engines which has a very similar geometry to those of real-size production engine injectors. Simultaneous visualization of two planes using high-speed and high-resolution CCD cameras has identified different types of cavitation, as well as their onset and development at different operating conditions. The flow configuration and experimental techniques used in the present investigation are described in the following section, followed by results and a summary of the main conclusions.

EXPERIMENTAL SETUP AND INSTRUMENTATION

INJECTION NOZZLE GEOMETRY

The use of an enlarged 3-D transparent model of the nozzle injector is essential due to the difficulty of examining the flow in real-size production systems. The present investigation focuses exclusively on a six-hole mini sac type nozzle for second-generation gasoline direct-injection engines. The six holes are symmetrically positioned around the nozzle tip 'dead' volume, each one of them at an angle of 45° to the injector axis, as can be seen in Figure 1, forming an overall spray cone angle of 90°. All the dimensions of the prototype real-size multi-hole nozzle were enlarged by a factor of 29 and the transparent model, shown in Figure 2, was manufactured from an acrylic material with a refractive index matching of 1.49. Three-dimensional views of the transparent model are presented in Figure 2.

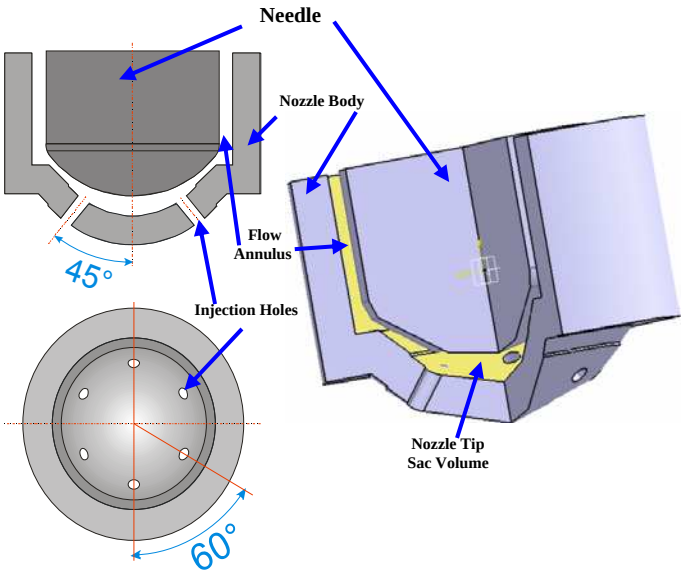

Figure 1: Geometry of the 6-hole fully symmetric injection nozzle.

The diameter of the real-size cylindrical injection holes with filleted edges was 140μm featuring a 0.2mm fillet radius and an overall length of 0.3mm. These values correspond to a nominal hole diameter and length of 4.1mm and 8.7mm, respectively, in the large-scale model. This resulted in a length-to- diameter (L/D) ratio of 2.12. The enlarged nozzle has been designed in a closed flow circuit configuration and, in order to minimise any back flow effects, the flow from the injection holes was entering into expanded by a factor of 3 flow holes connected to tubes leading to the suction pump. This design makes it possible to shape the nozzle body as a block with flat outer surfaces which offer advantages for imaging and laser measurement purposes.

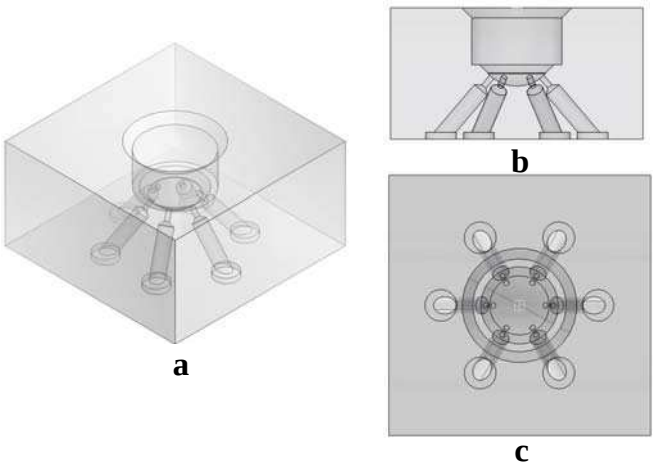

Figure 2: Three-dimensional models of the large-scale 6-hole nozzle; (a) isometric view of Perspex nozzle, (b) front and side view and (c) bottom view.

For dynamic flow similarity, not only it was necessary to model the geometry of the real-size nozzle injector, but also the geometry of the flow passages inside the injector upstream of the nozzle (Figure 3). This task was accomplished by enlarging the real-size geometry downstream from the needle shoulder, with the exception that the length of the flow passage along the needle was shortened slightly due to overall size limitations. Nevertheless, this has allowed the flow inside the enlarged needle annulus to be fully developed before reaching the nozzle annulus. The model was fixed in place by two metal flange-clamping mechanisms with O-rings between the flange and the acrylic nozzle body to provide sufficient sealing. The end part of the needle within the nozzle injector was also made of acrylic to enhance the optical access (see Figure 3).

ENLARGED INJECTOR TEST-RIG

A schematic overview of the experimental set-up with the incorporated large-scale model injector is shown in Figure 4. The use of the delivery and suction pumps, combined with the fact that it is a closed loop flow circuit, results in a modest fluid temperature rise. To compensate for this, a closed loop cooling serpentine was installed in the 90lt storage tank. A temperature controller, responsible for the flow control of the cooling fluid, ensured that its temperature was kept constant at around 25°C. A stirrer, installed in the storage tank, was used to provide thorough mixing, avoiding any steep temperature gradients in the working fluid. This approach guaranteed that the temperature- sensitive properties of the working fluid, like its density, kinematic viscosity, vapour pressure and surface tension, were all maintained constant at all times. The flow rate of the large-scale injector was primarily controlled by the variable speed pumps over a wide range. Further fine adjustment of the flow rate was achieved by means of the various flow and bypass valves installed. Accurate measurement of the overall flow rate was provided by an ultrasonic flow meter installed upstream of the large-scale injector in a fixed-length feed pipe.

The three-dimensional nozzle model provides the individual pressure measurement locations for accurate monitoring of the inlet, needle seat and outlet pressure values. Inlet and outlet pressures are of great importance in such experiments and can be adjusted independently by restricting the inflow and/or outflow of the injector. In order to reach sub-atmospheric outlet pressures and, therefore, simulate cavitation numbers of interest, a variable speed suction pump was installed in addition to the main feed pump. This made the investigation of the flow conditions at higher cavitation and Reynolds numbers possible.

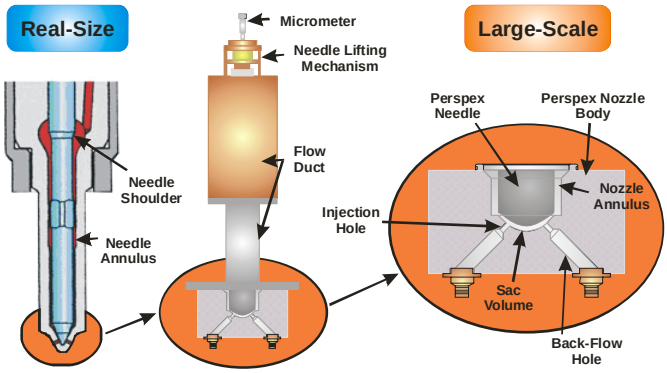

Figure 3: From real-size to large-scale injector.

The experimental set-up is effectively a steady-state flow test rig for in-nozzle flow visualisation purposes. This implies that the dynamic phenomena present under real operating conditions, due to the needle opening and closing events, are unrepresented. The needle was fixed to a certain lift simulating the desired real-size needle lift condition and was positioned manually by the needle lift mechanism; a micrometer was used to provide the exact position of the enlarged needle. The actual lift in the large-scale model is also scaled-up according to the enlargement factor of the injector nozzle. Water was used as the working fluid and thus, due to its refractive index of 1.33, some light distortion at the liquid-solid interfaces was expected; however, this would not affect the conclusion of the present investigation since the objective of this work was to visualise the full cavitation process using a continuous light source.

The liquid flow through the injector multi-hole nozzle, and especially through its holes, is known to be highly turbulent [3, 6, 7]. Although the experiment was run under steady-state conditions, all flow features and, in particular, cavitation in the injection holes, are expected to behave transiently and to have short time scales. This behaviour is virtually impossible to capture with conventional imaging (CCD camera) techniques. Since it is important to gain knowledge about the dynamics of cavitation inception and development for various flow conditions, a high-speed digital video technique was employed for this study.

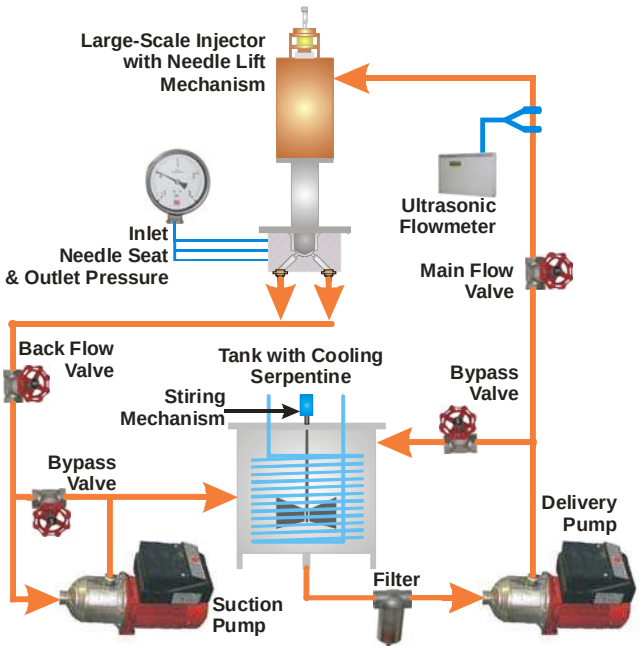

Figure 4: Schematic of the large-scale injector test rig.

HIGH-SPEED DIGITAL VIDEO TECHNIQUE

To capture the development of the cavitating flow inside the enlarged nozzle, a high-speed digital video system (Photron ultima APX) was set up in conjunction with the enlarged injector test rig. Two 10-bit video systems were used (mega-pixel Photron ultima APX) capable to take between 60 and 2,000 frames per second at the full resolution of 1,028 x 1,028 pixels. Higher framing rates of 3,000 up to 120,000 frames per second were possible at progressively reduced resolution. A strong halogen floodlight together with some halogen spotlights provided sufficient light for the non-intensified CCD imaging chip even at the highest used frame rates. The camera was operated by its control unit, which in turn was controlled by special software installed on the image collection computer. The software was responsible for programming critical operating parameters such as the desired frame rate, exposure time and triggering signals. Unlike other high-speed digital video systems, this system allowed the operator to set the shutter speed independently of the desired frame rate. All obtained images were saved at the image buffer, located in the camera's control unit, and downloaded onto a computer via a high-speed cable connection.

Two planes of the nozzle hole were imaged by the two high-speed cameras which were synchronised by interconnecting their control units so that images can be obtained at exactly the same time. This important feature allows for the simultaneous imaging of the area of interest from two different viewpoints, providing a better understanding of the three-dimensional flow patterns present in the nozzle.

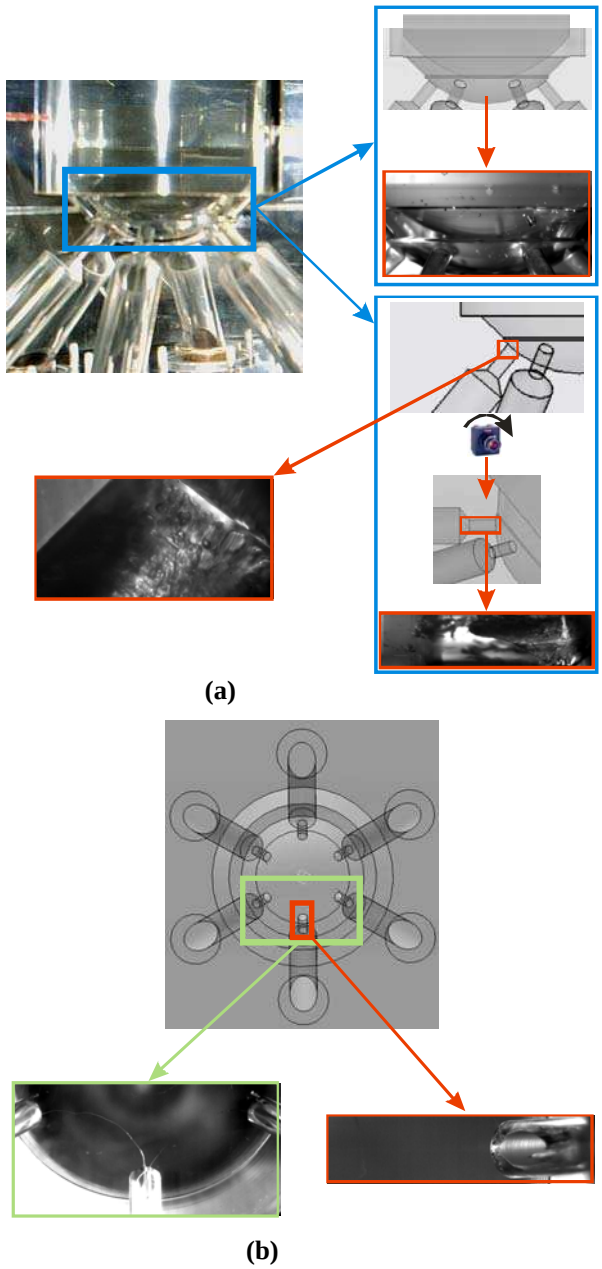

Figure 5: Schematic of imaging areas from (a) side-view and (b) bottom view.

The first camera was set to provide a side view of the model, while the second camera was installed below the large-scale nozzle in order to image the bottom view of the 3-D model. In Figure 5, a schematic of the side and bottom camera imaging areas and view angles is presented. Three different viewpoints were selected, in an attempt to fully characterise the flow patterns. The first viewpoint (r-h-s top in Figure 5(a)) includes all injection holes visible from the front view of the model, four holes in total, sac annulus and the volume around the needle tip. Although some light distortion is evident, due to the use of water as working fluid and the mismatch in the refractive indices of the material and the internal fluid, this view was selected with the purpose of demonstrating the flow streamlines by seeding the flow through the nozzle with tiny air bubbles.

The second and most important plane-view is focusing in one of the holes and can be seen in the r-h-s bottom of Figure 5(a). Since the flow velocity in the nozzle

holes is high, an increased framing rate is required in order to fully capture the cavitation development. In order to maximise the frame rate while maintaining sufficient cavitation image resolution, the camera was aligned relative to the orientation of the injection hole, which forms a 45° angle to the injector axis. Therefore, the camera was rotated almost 45° and the resulting image represents a horizontal cross-section of the injection hole. This camera viewpoint was selected for synchronisation with the second, bottom camera, which was also set to image the same injection hole.

The third plane-view, Figure 5(b), focuses on the cavitation structures present in the injection hole as viewed by the second camera which could provide two different bottom views of the nozzle model. The overall view (l-h-s image in Figure 5(b)) includes the flow in the sac volume region and three of the injection holes, while the r-h-s image focuses exclusively on the same injection hole as that imaged by the side camera, providing two synchronised images.

In this experiment the main frame rate was set at approximately 15,000 frames per second, and varied according to the velocity field in each of the imaged areas. Higher frame rates were not selected due to limitations in image resolution At the same time, due to the sufficient lighting provided, exposure times were kept as minimum as possible. Typical exposure times of 1/50000s, or 20μs, provided sufficiently sharp images, since the relevant transient phenomena were of medium speed rate. It should be noted that the software used provided several choices with regard to the output image format. Colour-based information is not lost but a conversion to greyscale was needed, from linear to logarithmic, for the dark areas to be shifted towards higher intensity values while maintaining the already light areas almost untouched. Effectively, the conversion of a linear greyscale to logarithmic alters the gamma (γ) value of the colour map. This is the safest way of adjusting the brightness of an image without neglecting critical information hidden in the pixel intensity values. Following the colour map correction, the data images had to be masked for covering background light reflections that severely affect the contrast; higher contrast is translated into a sharper and more detailed image. All the image processing was done through the development of in-house custom-made software using the Matlab platform.

EXPERIMENTAL RESULTS

Investigations of cavitation inside large-scale three-dimensional model nozzles of gasoline high-pressure injectors can provide useful information for improving the physical understanding of nozzle cavitation, its dependency on parameters such as nozzle geometry and flow conditions, and its link with spray characteristics. Representative images of in-nozzle flow patterns and the various forms of cavitation are presented here. The steady-state flow conditions examined, in terms of flow rates and pressure variations at fixed needle lifts, correspond to needle lifts of 1/4, 1/2, 3/4 and full lift (see Table 1). Dynamic similarity between the enlarged and real size injectors was established by matching the corresponding flow Reynolds numbers; however, matching of the cavitation number proved impossible as the pressure drop across the nozzle injector was much higher in the case of the real size injector. Fixing the needle lift imposed another departure from real size injector operation, as it was not possible to represent the dynamic flow phenomena associated with the needle opening and closing events. However, the investigations reported in [3,7] showed that, despite these discrepancies, the similarity of the cavitation structures formed in the enlarged and real size injectors was quite remarkable. As shown in previous studies, nozzle cavitation in diesel injectors has its origin in areas of low local pressure which are found either in the core of the recirculation zones formed in the upper corner of the injection hole inlet or in mean flow vortical structures.

INTERNAL NOZZLE FLOW PATTERNS

A first step towards better understanding of the phenomena that take place inside the nozzle of high-pressure gasoline injectors is a simple flow mapping for effective visualisation of the dominant flow patterns. There are various ways of achieving high-quality visualisation and extracting flow streamlines derived from images. Most of the techniques used are based on flow seeding using various solid or other lightweight particles (flakes) which are neutrally buoyant to the carrier fluid. Unfortunately, the nature of the large-scale model test rig prohibits the use of metal or plastic flakes for effective flow seeding. It was thus decided that the best solution was the use of air bubbles which were introduced into the flow upstream of the enlarged injector through a small nozzle. Although air-bubbles are not an ideal choice for marking the water flow, their use has provided useful information on the large-scale mean flow patterns present in the sac volume (see Figures 6-8).

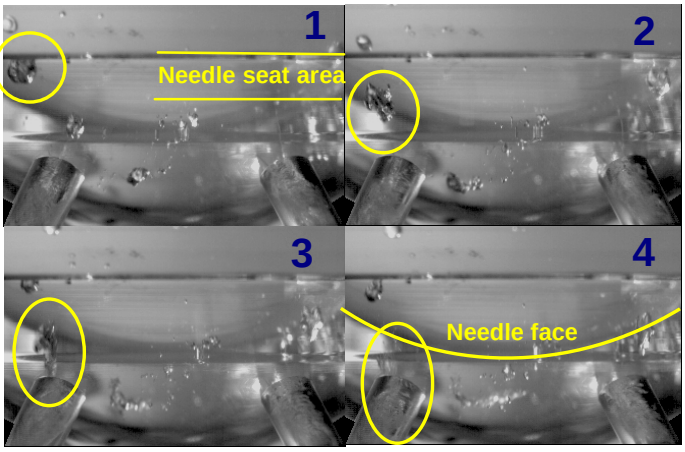

Figure 6: Image sequence demonstrating primary inlet flow to the injection hole.

The selection of the seeding medium proved quite efficient but the results may not accurately represent the expected flow patterns due to the large size of the air bubbles and associated buoyancy effects. In the case of multi-hole nozzles, access to the holes comes from the annular flow upstream which, after passing the needle seat area, seeks the easiest way-out through the nozzle

where the pressure is lowest. As it can be seen from the sequence of high-speed images presented in Figure 6, the air bubble, marked by a yellow circle in image number 1, is located directly upstream the injection hole as it crosses the needle seat area. In the next two images (numbers 2 and 3) the deformation of the bubble shape is evident, due to the mean flow gradient and turbulence associated with the low-pressure area introduced by the hole inlet further downstream. The bubble was finally convected into the injection hole and by image number 4 has already disappeared.

There are six injection holes in the investigated nozzle and, based on the previously presented findings, it is important to identify the flow patterns around the entire flow annulus and sac volume. Since the nozzle design is axis-symmetric, the area of interest would then be the region in-between two adjacent injection holes. As liquid passes through the needle seat area, there is no apparent exit on its way, except for a strong velocity gradient initiated from the low-pressure regions at the two neighbouring injection holes. The flow is then directed towards the closest hole by changing its initial direction and creating a secondary inlet flow towards the injection holes. Figure 7 demonstrates the above described flow behaviour. At the middle point of the inter-hole distance, the liquid faces strong shear forces associated with the equally strong pressure gradients. The marked bubble in the image sequence presented in Figure 7 starts to split as it approaches the injection holes, image number 2. Initially it forms two elongated groups of bubbles but, as it maintains its momentum, the bottom part is further detached forming effectively the third and smaller group of bubbles observed in the fourth image of the sequence. The left and right circles, in image number 5, mark the bubbles that turn towards the left- and right-injection holes, respectively, forming the side entry flow for these holes. The bottom part of the initial bubble is not dragged towards any of the two injection holes, since it has passed the high-pressure gradient area due to its momentum. As illustrated in the last image of the sequence, this latter part of the bubble continues its way downstream where it finally reaches the bottom of the nozzle sac volume where it interacts with the flows coming down from the other inter-hole spaces.

Liquid trapped in the sac volume seems to be mainly stagnant, as shown in Figure 8. The flow from the sac volume to the exit holes (bottom inlet flow) has very low velocity and its contribution to the total inlet flow is rather small. Figure 8 shows a bottom view of the nozzle model including two injection holes where, effectively, only a portion of the nozzle sac volume is visualised. In this high-speed image sequence, a fine bubble is marked by the yellow circle. As the flow passes in-between the two visible injection holes, it is directed towards the sac volume. Images number 3 and 4 were taken at a time interval of 1ms; this time scale provided sufficiently long time to visualise any movement in the highly transient flow field of the injector nozzle. It is apparent from these images that there is not any defined movement of the marked bubble and the flow can be considered to be stagnant.

In order to identify and understand the dynamic behaviour of the various cavitation structures under different conditions, the enlarged injector test rig with the transparent multi-hole model nozzle was operated at different flow conditions and needle lifts.

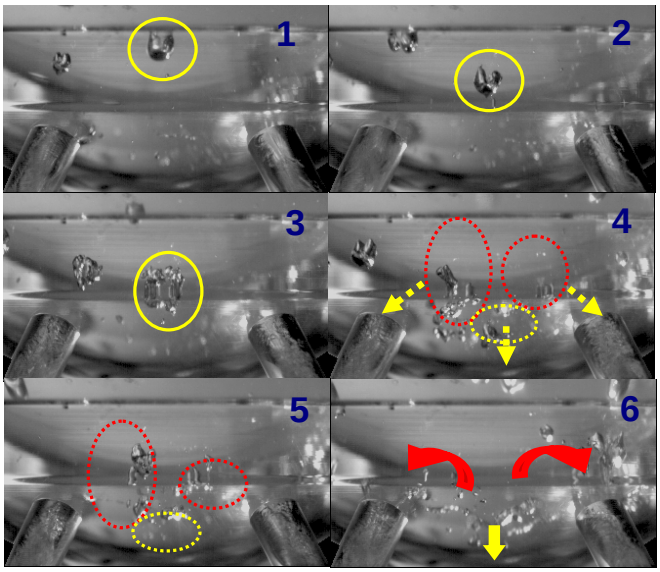

Figure 7: Image sequence demonstrating flow splitting in-between two injection holes.

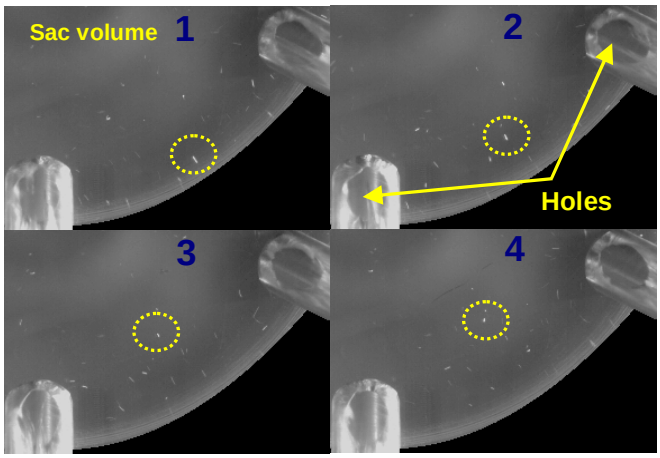

Figure 8: A sequence of images demonstrating the short timescales of the flow in the sac volume.

All experimental test conditions are listed in Table 1, where P_{inj} is the absolute static inlet pressure, P_{back} is the absolute static outlet pressure and U_{inj} is the bulk velocity of the flow through an injection hole calculated as $Q_t/6A$ where A is the nozzle hole cross-sectional area and Q_t is the total flow rate through the model injector. The examined fluid flow and pressure conditions are aiming to cover the equivalent range of low loads in terms of the cavitation numbers and low-to-high loads in terms of the flow rates through the nozzle for a real-size injector used in modern direct-injection spark-ignition engines. Matching cavitation numbers greater than 5, which represents the minimum value under realistic injector operating conditions in an engine, proved not to be feasible with the existing large-scale model test rig for the reasons given above. On the

other hand, the existing set-up could operate at a range of Reynolds numbers between 30,000 and 72,000.

Needle Lift = 0.51mm (1/4 of the full lift)						
CN	Re	P_{inj} [bar]	P_{back} [bar]	U_{inj} [m/s]	Flow Rate Q_t [l/s]	Frame Rate [1/s]
4.00	52614	3.60	0.75	12.88	1.03	15000
4.22	61899	4.75	0.95	15.15	1.20	15000
4.57	37139	2.00	0.40	9.09	0.75	15000
4.72	49519	3.20	0.60	12.12	0.97	15000
5.00	30949	2.55	0.46	7.57	0.65	15000
5.20	34044	1.62	0.30	8.33	0.67	15000
Needle Lift = 1.02mm (1/2 of the full lift)						
CN	Re	P_{inj} [bar]	P_{back} [bar]	U_{inj} [m/s]	Flow Rate Q_t [l/s]	Frame Rate [1/s]
2.40	34044	1.43	0.45	8.33	0.69	15000
3.00	34044	1.43	0.39	8.33	0.69	15000
3.22	40234	1.75	0.45	9.85	0.80	15000
3.75	61899	3.78	0.85	15.15	1.15	15000
Needle Lift = 1.53mm (3/4 of the full lift)						
CN	Re	P_{inj} [bar]	P_{back} [bar]	U_{inj} [m/s]	Flow Rate Q_t [l/s]	Frame Rate [1/s]
1.00	43329	2.00	1.02	10.60	0.82	15000
1.50	46424	2.34	0.96	11.36	0.90	15000
1.70	46424	2.34	0.90	11.36	0.90	15000
2.00	30330	1.42	0.50	7.42	0.60	15000
2.40	30330	2.25	0.70	7.42	0.60	15000
3.00	30330	2.25	0.60	7.42	0.60	15000
3.20	30330	2.15	0.55	7.42	0.60	15000
3.50	58804	3.20	0.75	14.39	1.14	15000
Needle Lift = 2.04mm (Full lift)						
CN	Re	P_{inj} [bar]	P_{back} [bar]	U_{inj} [m/s]	Flow Rate Q_t [l/s]	Frame Rate [1/s]
0.62	37139	2.40	1.50	9.09	0.75	15000
0.73	37139	2.30	1.35	9.09	0.75	15000
0.78	37139	2.20	1.25	9.09	0.75	15000
0.89	37139	2.05	1.10	9.09	0.75	15000
1.00	58803	3.30	1.63	14.39	1.14	15000
1.27	58803	3.30	1.48	14.39	1.14	15000
1.50	49519	2.50	1.03	12.12	0.97	15000
1.50	58803	3.30	1.35	14.39	1.14	15000
1.70	49519	2.50	0.96	12.12	0.97	15000
1.70	58803	3.30	1.25	14.39	1.14	15000
2.00	37139	2.12	0.74	9.09	0.75	15000
2.00	58803	3.30	1.13	14.39	1.14	15000
2.40	37139	1.77	0.55	9.09	0.75	15000
2.40	58803	3.30	0.99	14.39	1.14	15000
2.70	37139	1.75	0.51	9.09	0.75	15000
3.00	49519	2.20	0.59	12.12	0.97	15000
3.00	58803	3.30	0.86	14.39	1.14	15000
3.00	72731	5.00	1.29	17.80	1.40	15000
3.20	37139	1.52	0.40	9.09	0.75	15000
3.20	58803	3.00	0.75	14.39	1.14	15000

Table 1: Flow conditions inside the large-scale multi-hole nozzle for needle lifts from a quarter to full.

The selection of four different needle lifts is based on an attempt to parametrically study the in-nozzle cavitation phenomena and their behaviour under the widest possible range of flow conditions. Unfortunately, in real engine applications, it is not possible to vary the needle lift as a function of the engine's fuel requirement. Therefore, although a parametric study based on various needle lift positions does not simulate closely any realistic engine operation, it is nevertheless very helpful for the investigation of cavitation and its dependencies on flow conditions. The values of the Reynolds number and the cavitation number listed in table are calculated according the below definitions;

$$\mathrm{Re} = \frac{D \cdot U_{inj}}{\nu_L}$$

and

$$CN = \frac{p_{inj} - p_{back}}{p_{back} - p_{vapour}}$$

where D is the nozzle hole and ν_L is the liquid kinematic viscosity.

INCEPTION OF CAVITATION

Observation of the flow in the large-scale multi-hole nozzle has revealed that increasing the cavitation number resulted in the formation of different types of cavitation. All of the investigated conditions confirmed that cavitation behaviour in the enlarged nozzle was highly dynamic and unstable. Initially and unexpectedly, a 'needle string' was identified prior to any evidence of hole cavitation. It is termed 'needle string' since it appears to originate at the needle surface facing an injection hole and to extend downstream inside the hole. At very low cavitation numbers, of the order of 0.5-0.7, strings originating at the needle surface extended downstream into the hole when the process was fully developed, as can be seen in Figure 9 top row. The occurrence of such strings is quite random and can happen to any one of the nozzle holes. There is evidence that needle strings are created at the core of the instantaneous vortical flow structures which extend from the nozzle hole axis towards the section of the needle surface with the lowest local pressure, due probably to the adverse pressure gradient as the flow turns following the curvature of the needle tip. It can be argued that the slightest geometric eccentricity of the needle due to a manufacturing imperfection can promote the formation of a vortical structure in the sac volume; this effect is not significant in the present enlarged nozzle geometry which is axisymmetric with a concentric needle.

To trace the development of the needle string from the needle surface to the nozzle hole, additional side-view images of the flow were taken to include both the in-nozzle and sac volume flows; this sequence of images is shown in Figure 10 where the imaging area was increased at the expense of lowering the framing rate to 12,500 frames per second. Above the nozzle hole entrance and prior to the needle seat area, as a result of the conical curvature of the model, severe optical distortion was observed which necessitated an insert with the same background colour to be introduced in all the images. The obtained images clearly show the inception of needle cavitation close to the needle surface (indicated by a yellow circle in the second image) and its gradual growth towards the centre of the opposing hole. Some 0.3 ms after the initiation of the string, it enters the nozzle hole and continues to move forward inside the hole. The results at all measurement

conditions revealed that this type of cavitation collapses before reaching the exit of the nozzle hole which suggests that its influence on the spray structure and stability may not be significant.

It is also evident that, once the needle string is inside the hole, its convection towards the exit is very slow, according to the time sequence of Figure 10. This mechanism becomes more dominant as the needle lift decreases. Thus, at lifts lower than full needle lift, the flow field is modified due to the extensive throttling at the needle seat area and the reduced distance between the needle surface and the hole inlet, which result in sustainable needle string structures that are present at all times. With an increasing cavitation number, needle strings tend to disappear mainly due to the flow field modifications imposed by hole cavitation that appears around the injection hole inlet. Further increase in the cavitation number causes needle strings to be replaced by in-hole cavitation strings, as will be described in following sections.

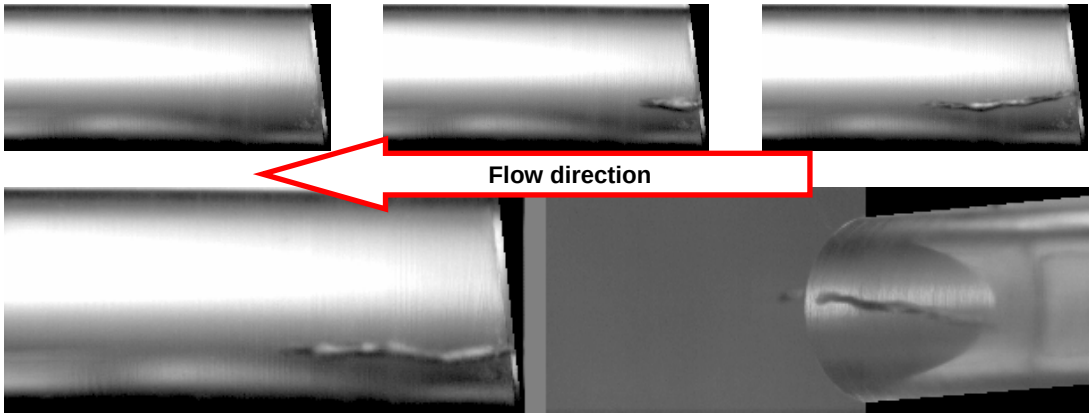

Figure 9: *Top row*; Images of 'needle string' development. *Bottom row*; combined side and bottom view images of a 'needle string' obtained simultaneously.

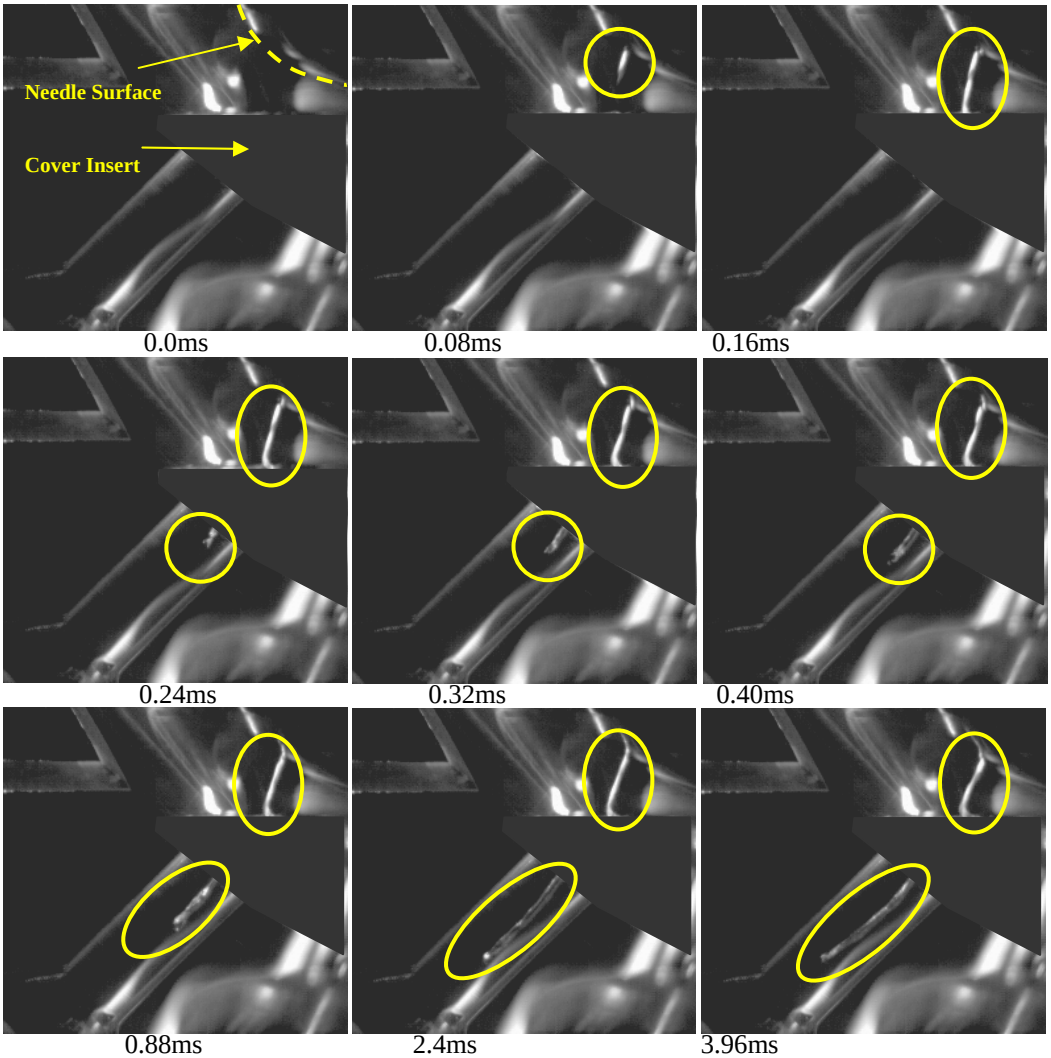

Figure 10: Side-view sequential images of 'needle string' development at full needle lift and CN=0.55.

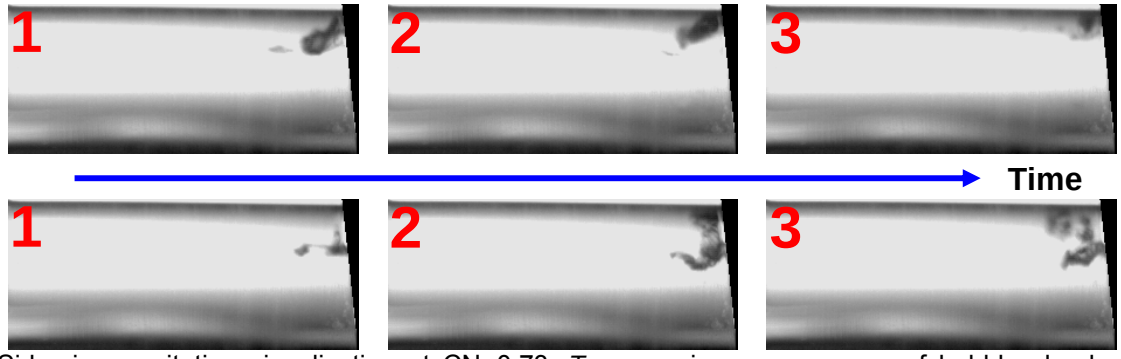

Figure 11: Side-view cavitation visualisation at CN=0.73. *Top row*; image sequence of bubble cloud at upper hole corner. *Bottom row*; interaction between needle string and hole cavitation.

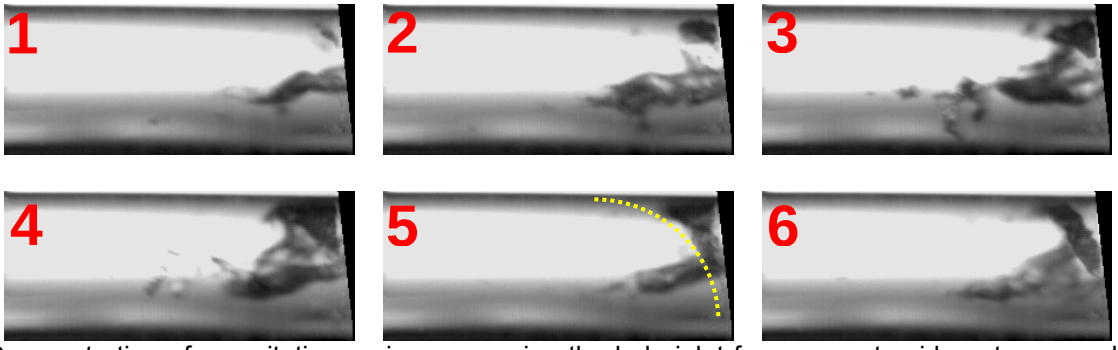

Figure 12: Demonstration of a cavitation regime occupying the hole inlet from upper to side entrance walls at CN=0.9 and full valve lift.

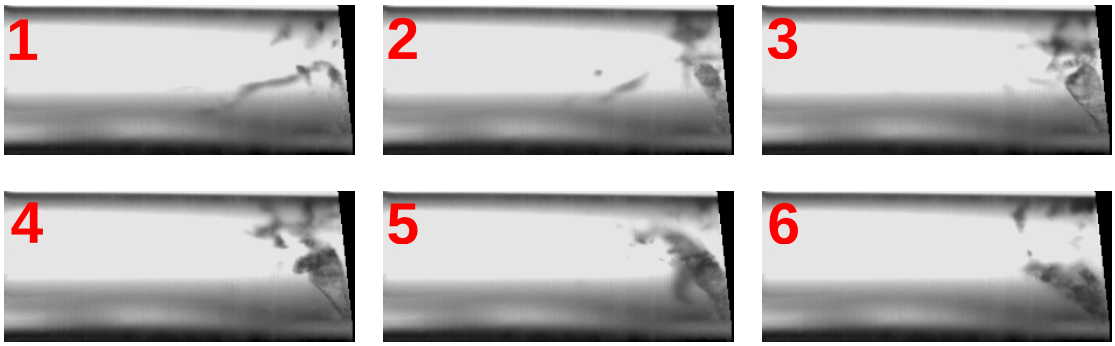

Figure 13: Image sequence demonstrating cavitation at the side entrance walls at CN=0.9 and full valve lift.

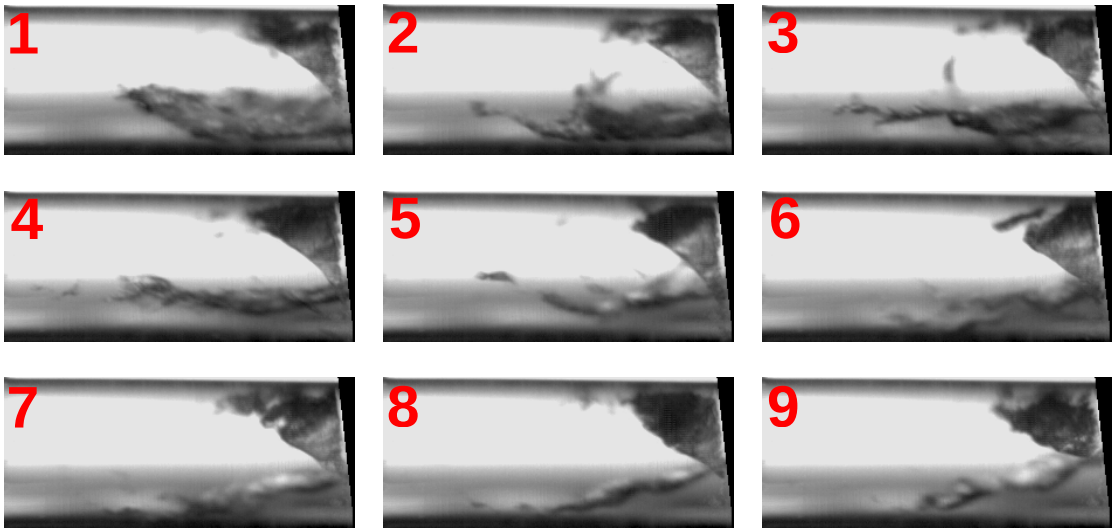

Figure 14: Image sequence of canopy shaped cavitation film development at CN=0.9 and full valve lift.

If the cavitation number increases further, in the range 0.7-0.9, some bubble clouds start to appear in the upper hole corner (Figure 11 top row), while needle strings are still visible below them. These clouds are unstable and tend to detach from the hole surface quite frequently and to collapse further downstream in the nozzle hole. In the image sequence presented at the bottom row of Figure 11, the interaction between persisting needle strings and the bubble cloud in the upper hole entrance is clearly evident. A needle string structure could randomly move upwards and, as its low-pressure core approaches the upper hole inner surface,

it causes further pressure drop which leads to a bubble cloud appearing in that region. Overall, it seems that these are the two mechanisms responsible for the first appearance of cavitation in the nozzle holes of a multi-hole large-scale model injector.

As the cavitation number increases to values around 0.9, geometric cavitation develops in three different ways as shown in Figures 12, 13 and 14 at the same operating condition. The sequence of images in Figure 12 demonstrates how a cloud created in the upper hole corner can develop to occupy half of the hole entrance, forming a shape the follows closely the entry curvature of the hole. Needle strings, still visible at these cavitation numbers, do not seem to interfere with the formation and development of hole cavitation. In the first two images in Figure 12, it is clear how a small cloud is created at the top of the hole entrance, due to the low pressure region caused by the rapid turning of the liquid into the hole. In images 3 and 4, this cloud has taken a triangular shape and, ultimately, in the last two images it is shown to occupy almost half the hole entrance by following its curved perimeter.

Given the highly transient nature of the nozzle flow regimes, the aforementioned mechanism is not unique. As Figure 13 demonstrates, there could be cavitation inception at the sidewalls of the hole entrance in the absence of any cavitation regimes at the top entrance of the hole; this may suggest a non-uniform pressure distribution in the corner vortex at the inlet to the hole due to the complex and highly transient nature of the flow at the nozzle inlet, as shown in [7]. In Figure 13, the needle string present in the first images disappears and, in the absence of a stable cloud at the top of the hole, a group of bubbles appears at the sidewalls to form a cavitation film which is highly unstable and quickly collapses.

Finally, a more stable mechanism for forming cavitation films, that are canopy shaped and occupy most of the hole entrance perimeter, has been identified. This is presented in Figure 14 in a series of nine consecutive images. The relatively thin cavitation film, which is visible in the top right corner of each image in the sequence, occupies simultaneously most of the hole entrance perimeter and maintains its shape for longer times compared to the previously described top- or side-generated vapour films. The difference in light intensity gives a rough estimation of the vapour film thickness, although dark areas at the top of the film are due to the film present at the background wall of the hole.

DEVELOPMENT OF CAVITATION

In the large scale model the nozzle flow transitions from bubbly flow through pre-film to film stage cavitation, as identified in the high-speed videos, develop as a function of the cavitation number. For almost all investigated cavitation numbers, it seems that the cavitation structures are unstable due to the large pressure variations in the cavitation zones and the increased flow turbulence dominating the internal nozzle flow. From the sequential images, it can be seen that the flow entering the injection hole from the side, as well as the cavitation strings, play a major role in enhancing further cavitation inception and development. For cavitation numbers smaller than 1, it has been argued in previous sections that needle strings and bubble clouds represent incipient cavitation. As cavitation number increases to values equal and greater than 1, bubble clouds become more opaque and it is not possible anymore to distinguish between individual bubbles. Moreover, there is evidence at this point of bubbles beginning to coalescence into larger voids, which can give rise to the formation of local vapour films, as shown in Figure 15(a).

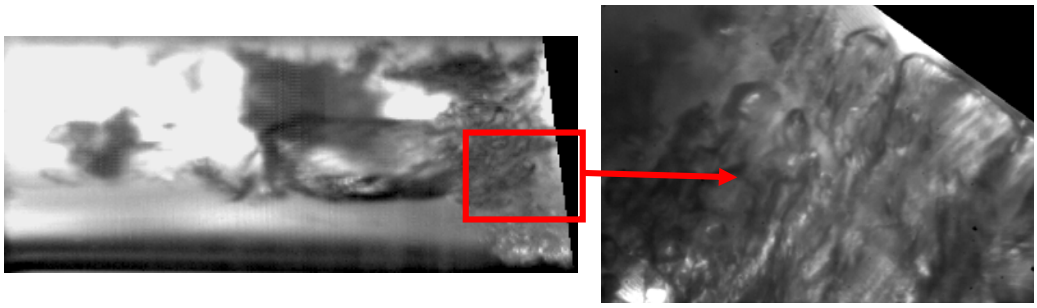

(a) Pre-film stage cavitation

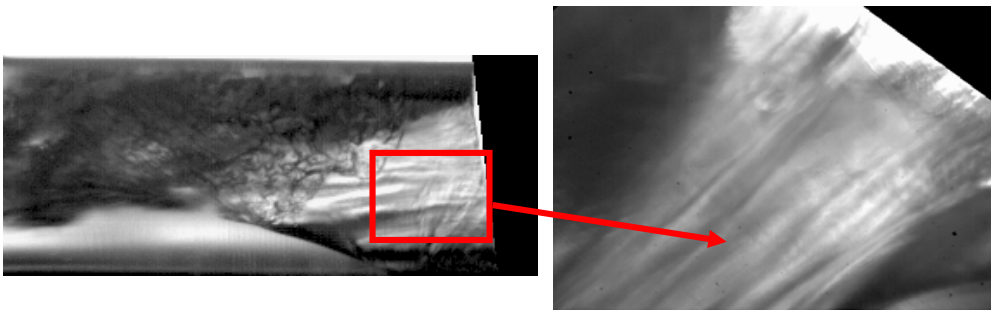

(b) Film stage cavitation

Figure 15: Cavitation regimes inside the 3-D large-scale model nozzle; (a) pre-film stage cavitation and (b) film stage cavitation.

A further increase of the cavitation number causes the flow to fully separate at the upper half of the nozzle hole inlet. This, in turn, induces the formation of a vapour film type cavitation, Figure 15(b), where the relatively thin film follows the curved shape of the hole. Although these geometrically induced cavitation patterns were found not to depend on the Reynolds number (flow rate), the development of these structures was strongly affected by the cavitation number. Almost identical trends in the behaviour of cavitation structures and their development has been reported in diesel injectors [3, 17]. It is also expected that surface tension scaling may influence the shape of the pre-film and film cavitation structures. For both most commonly used diesel nozzle configurations such as the Conical Mini-Sac and Valve Covered Orifice, similar pre-film and film stage cavitation structures have been reported. These structures seem not to depend on the Reynolds number, unlike the cavitation number and needle lift that both affect the transition between the different stages. The similarities in the internal nozzle flow between gasoline multi-hole and diesel injectors are of great significance since certain flow patterns of emerging gasoline multi-hole nozzles can be explained on the basis of previous results obtained in well established diesel nozzle geometries. They also imply some degree of independence of the internal nozzle flow on fuel properties.

Surprisingly enough, other string-type cavitation structures were observed to be present in the nozzle holes but their formation mechanism is radically different than that of the needle strings. Although the geometry of the examined nozzle is axisymmetric, a vortex structure was identified to be present in the volume between needle, needle seat and two adjacent holes. The vortex and string formation was attributed to the interaction between the high momentum annular flow and the cross flow induced by the intermittent throttling of individual holes which are cavitating already at their entry. As a result, the flow conditions at the vortex core lead to the formation of a low-pressure region and, subsequently, of cavitation bubbles. The bubbles coalesce immediately into a continuous vapour string along the core of the vortex as can be clearly seen in Figure 16. This string is formed inside one injection hole by a strong vortex around the hole axis, as shown in the image sequence of Figure 18, which then extends upstream into the hole inlet where it triggers a bubble creation mechanism at the core of the vortex between two adjacent holes. The succession of bubbles forms a fine string structure that, if strong enough, may extend into the neighbouring injection hole. These strings seem to develop transiently and intermittently between adjacent nozzle holes.

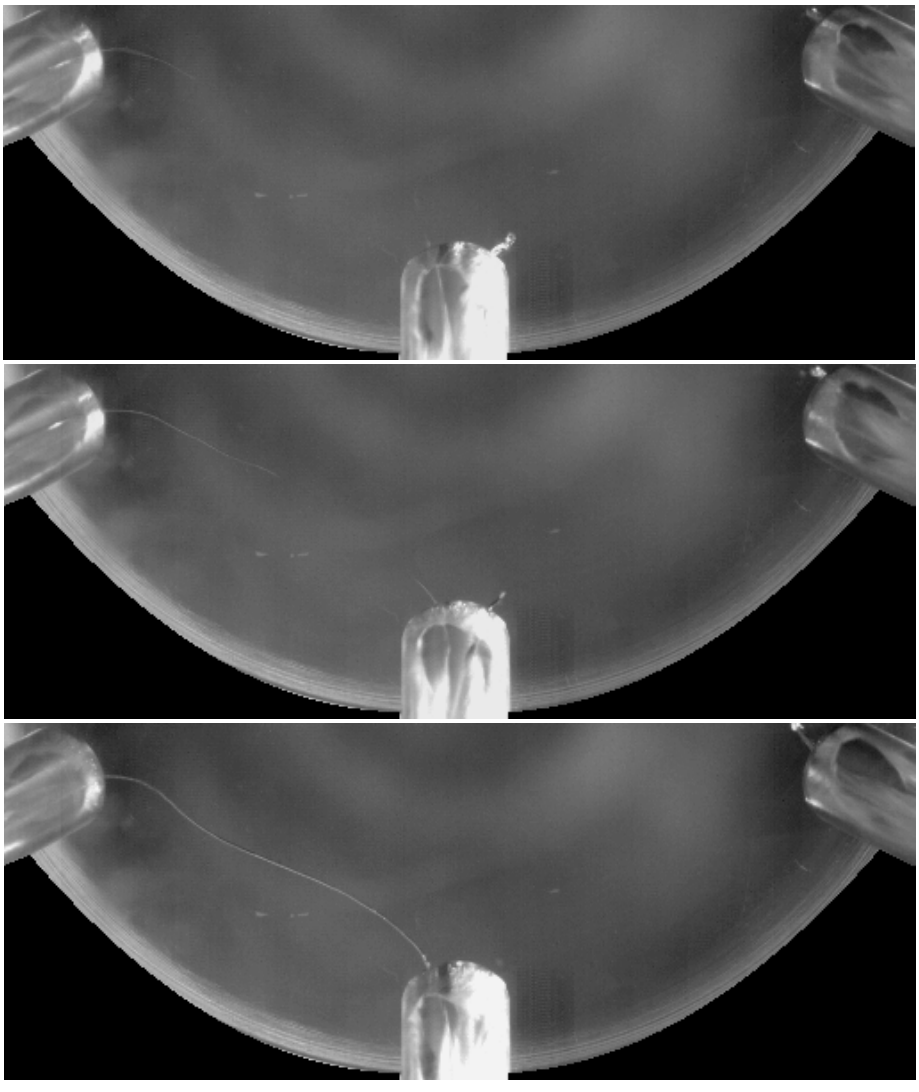

Figure 16: Image sequence of developing cavitation string between two adjacent needles.

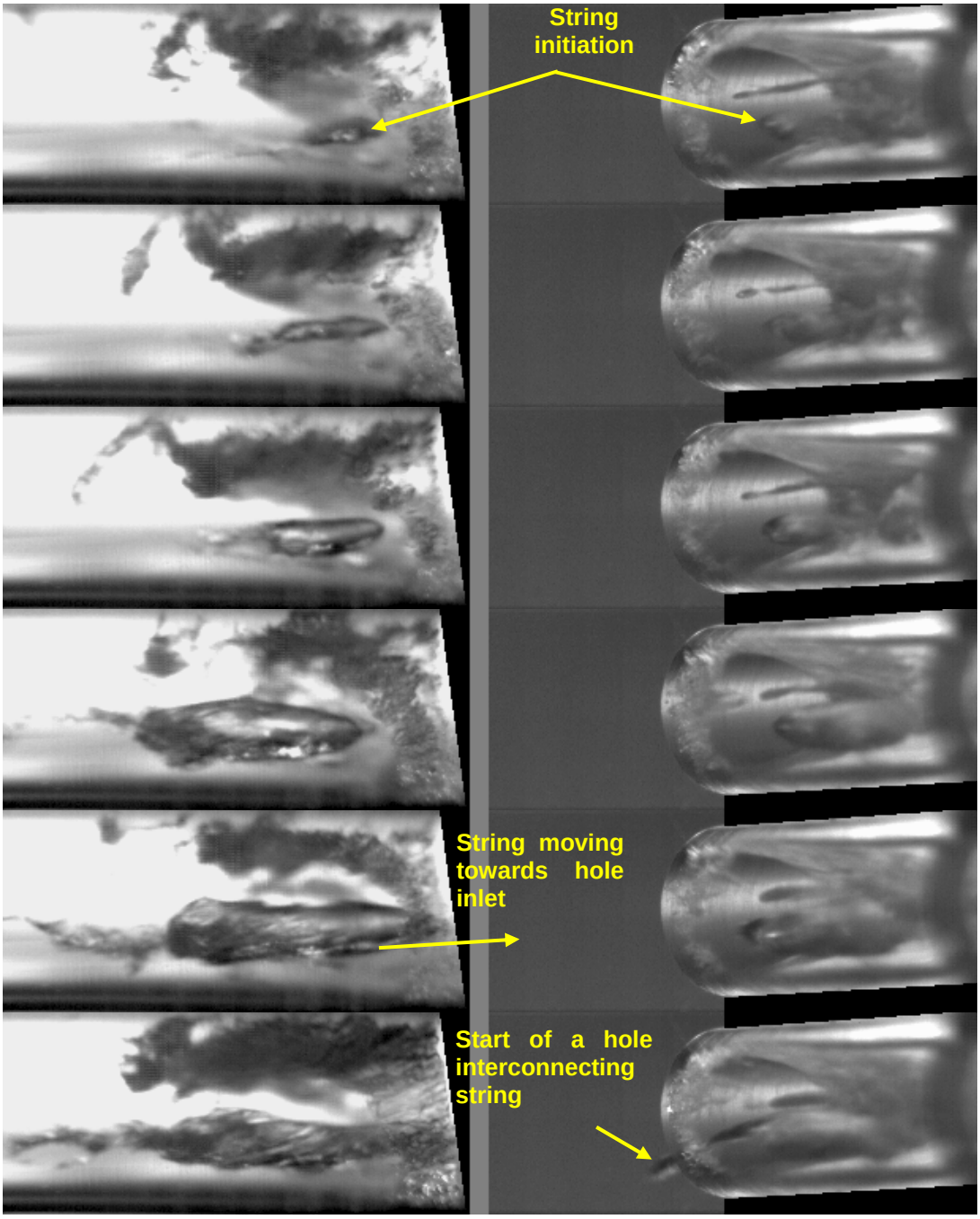

Figure 17: Sequential images presenting the mechanism of formation of a hole cavitation string at CN=1.

The same type of vertical flow structure is responsible for another form of string type cavitation, the so called 'vortex-cavitation'. This time, after the initiation of string cavitation in the nozzle hole, figure 17, the part of cavitation which moves downstream towards the exit of the hole is diffused into large conical clouds of bubbles, which then mix with the already established hole geometric cavitation structures, as a result of the high pressure, complex vortical flow and high turbulence in that region. What might prove to have major practical importance is the interaction of this vortex-cavitation inside the hole with the cavitation structures already formed in the upper region of the injection hole, which may give rise to turbulence enhancement and hole-to-hole variations in the two-phase mixture exiting the hole. Thus, despite the axisymmetric geometry of the vertical multi-hole nozzle, variations in the flow pattern between holes are likely to be present due to the complex two-phase flow present in the sac volume and holes after the onset of cavitation. The actual influence of the highly transient vortex-cavitation on the in-nozzle flow structures inside multi-hole nozzles at cavitation numbers of the order of 1 is presented in a sequence of high-speed video images in Figure 18.

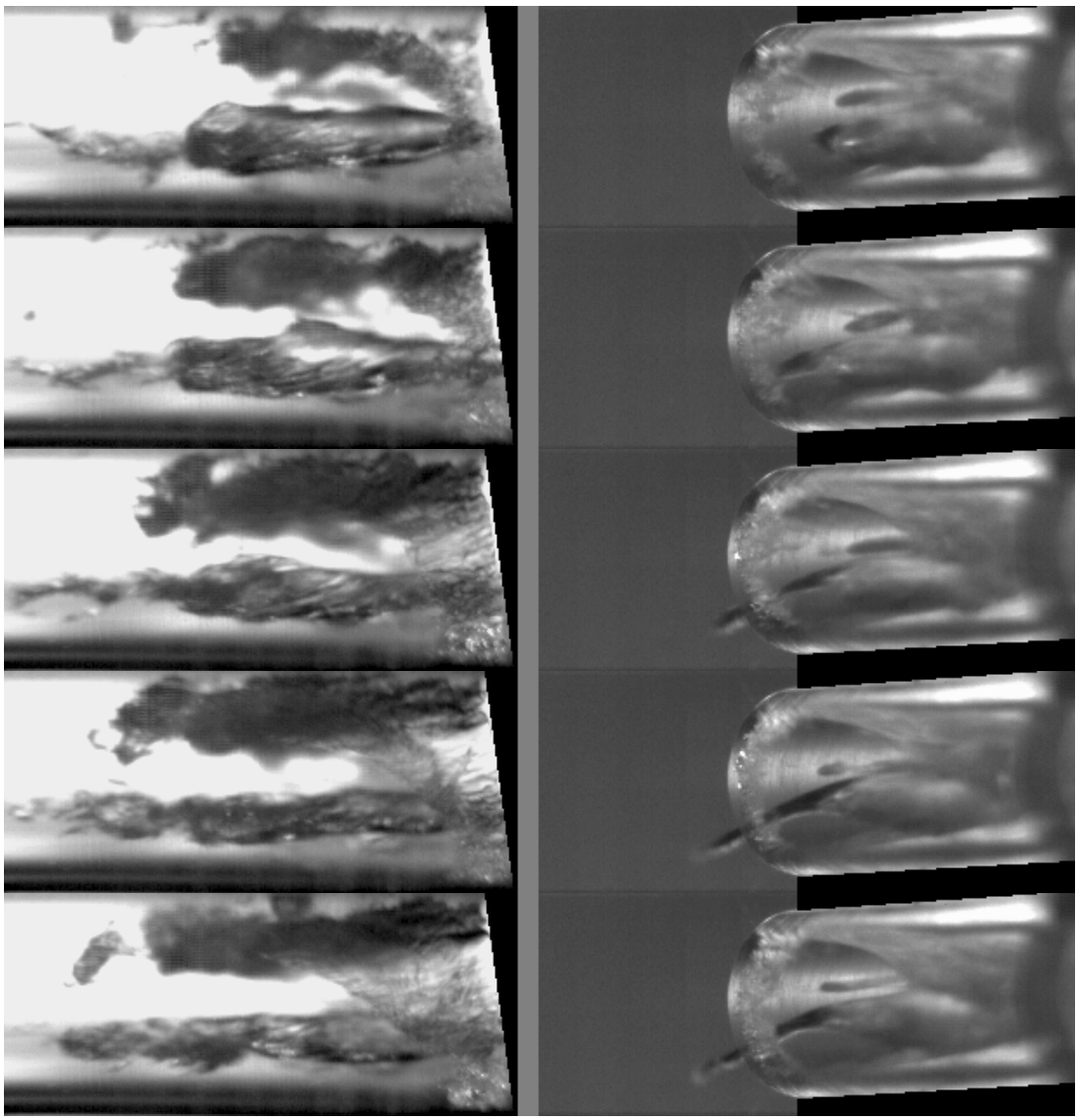

Figure 18: Interaction between a cavitation string and in-hole cavitation structures at CN=1.

In the first image of the above sequence it is clear that geometric cavitation around the hole inlet is unstable and not fully developed. At the same time, vortex-cavitation strings can be identified that do not extend up to the hole inlet, although later images in the sequence show that cavitation strings can been extended well beyond the hole boundaries. The vapour volume induced by the string reduces the effective flow area at the hole inlet and, in turn, fluid flow entering the hole is accelerated. A series of events are being triggered and the resulting flow acceleration is responsible for further pressure drop in potentially low-pressure regions. It can thus be argued that this leads to enhanced stability of the cavitation structure around the hole inlet boundary. As presented in the latter images of the above sequence, pre-film stage cavitation is well established and the detachment of the flow from the side hole walls is evident.

Pre-film stage cavitation has been clearly identified in high-speed video images for cavitation numbers up to 2. The main feature of the observed cavitation regimes has been their highly unstable structure and transient behaviour. More specifically, as cavitation number increases, film stage cavitation appears although it seems not to be well established unless the cavitation number exceeds 2. Therefore, as the image sequence in Figure 19 shows, there is continuous alternation between pre-film and film stage cavitation. The first images at this sequence present a bubbly cavitation pre-film, while in the latter ones the tendency for bubbles to coalesce and form a film structure is clearly evident. The above-described transient behaviour proved to be almost independent of the flow rate through the nozzle (Reynolds number), but highly dependent on the valve lift.

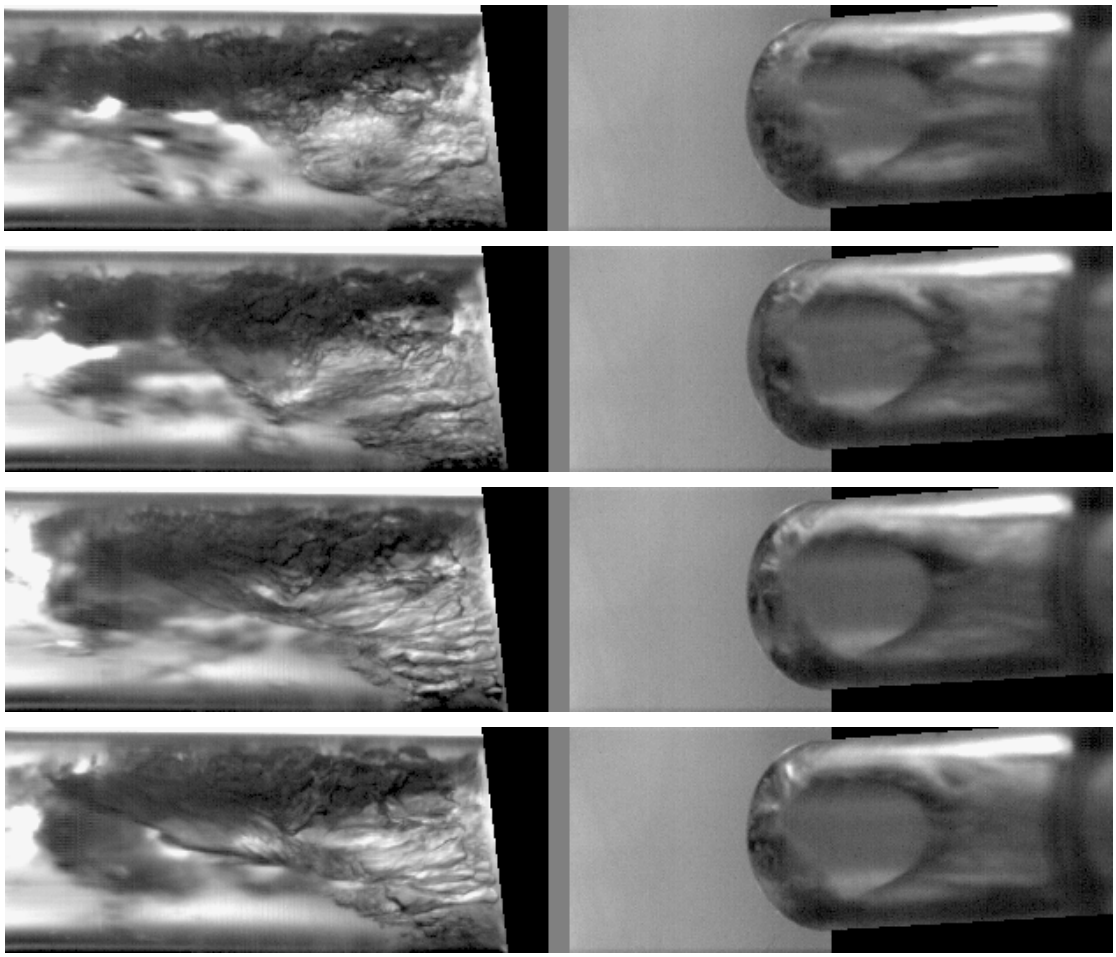

Figure 19: Alternation of pre-film to film stage cavitation at CN=2.

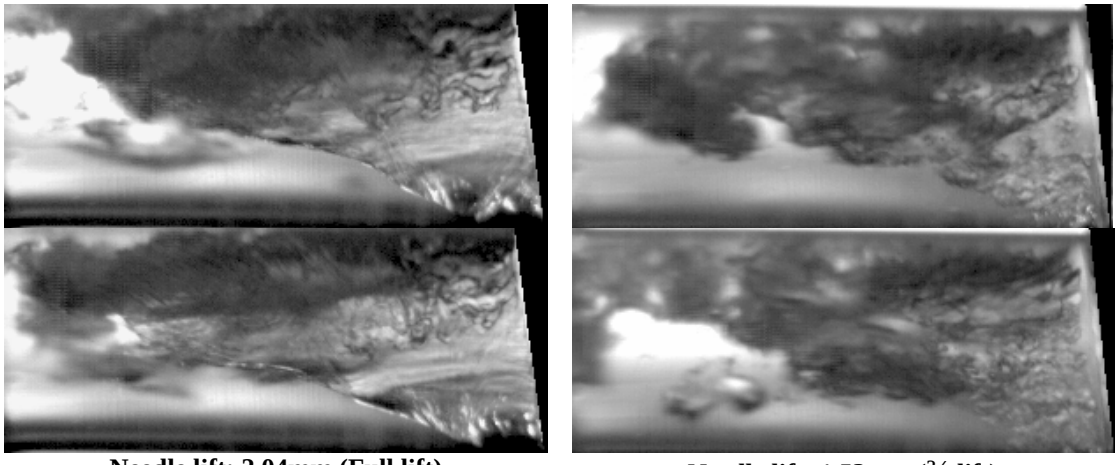

Needle lift: 2.04mm (Full lift) **Needle lift: 1.53mm (¾ lift)**

Figure 20: Effect of needle lift on cavitation structures (CN=1.5, Re~46,500, ~49,000).

Regarding the effect of needle lift on the cavitation pattern development, it was observed that a low needle lift leads to more turbulent flow behaviour and thus bubblier cavitation (r-h-s of Figure 20). Increasing the needle lift gives rise to a more stable flow and the cavitation structures inside the injection holes transform into a more or less steady cavitation film (l-h-s of Figure 20). A direct comparison could be seen in Figure 20, where all images were taken at a cavitation number of 1.5, a Reynolds number of 46,500 at full lift and 49,000 at the lower lift for two different needle lifts of 2.04 and 1.53mm. The difference in the film structure is visible and the turbulent bubbly flow induced by the lower needle lift is clearly identified in the right-hand-side column of the figure.

In addition to the previously discussed phenomena, a recirculation zone was identified throughout the

transitional period from pre-film to film stage cavitation. Given the unstable behaviour of both types of cavitation, bubbles that did not manage to integrate into the created film maintain their shape and attach to the hole side walls, thus allowing a kind of flow-seeding in that region. The flow inside the gaseous pocket that the detached cavitation film has created is almost stagnant and subject to pressure differences across that region. In some cases, the low-pressure at the hole entrance is adequate to create a small recirculation zone inside that gaseous pocket. An example of such behaviour is presented in Figure 21 where a small bubble marked by a red circle moves towards the hole entrance. In addition, another frequent flow structure inside the gaseous pocket that the cavitation film creates is presented in Figure 22. Here the flow moves upwards, from the bottom hole entrance wall towards the top hole wall, and it is mainly visible due to the texture of the interacting interface between gas and liquid.

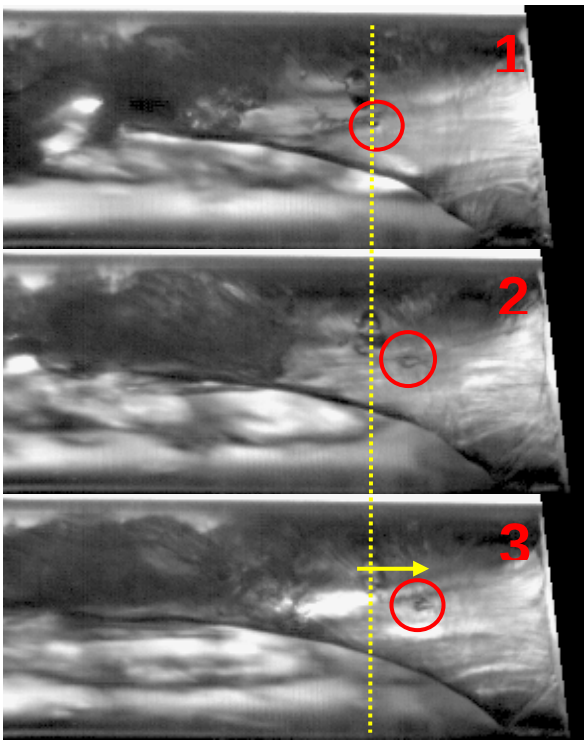

Figure 21: Representation of the recirculation zone inside the gaseous pocket of film cavitation at CN=2.5 and full valve lift.

At cavitation numbers higher than 2.5, film stage cavitation is well established and the film thickness is substantially larger than at any lower cavitation number. A representative example is presented in Figure 23 where the cavitation number is set to 3 and the thickness of the vapour cloud blocks the light from reaching the camera, thus appearing darker than in previous flow conditions. Furthermore, as cavitation number increases, vortex strings appear almost permanently in the injection hole and frequently develop into hole-to-hole interconnecting strings. Neither the film stage cavitation patterns nor the in-hole cavitation strings seem to depend on the Reynolds number. This was verified by keeping the cavitation number and needle lift constant at 3 and full lift, respectively, and varying the Reynolds number from 49,000 to 73,000. The results showed no major changes on both types of cavitation structure.

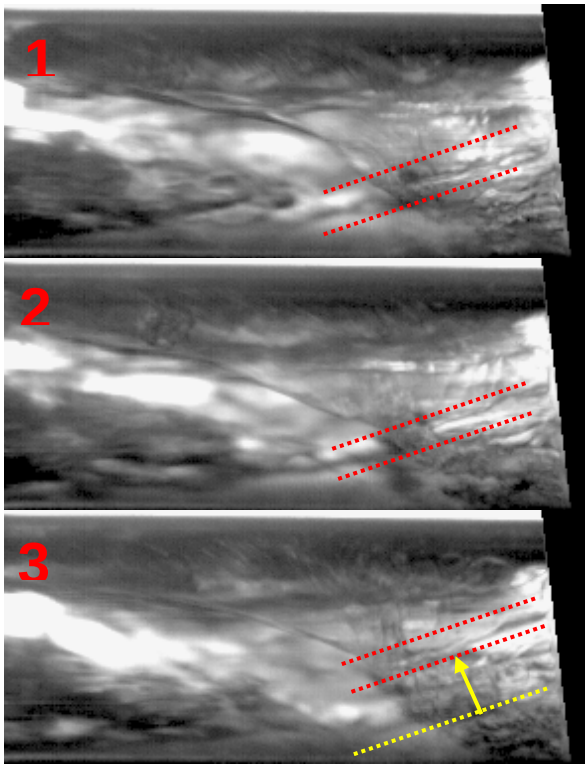

Figure 22: Flow structure inside the gaseous pocket of film cavitation at CN=2.5 and full valve lift.

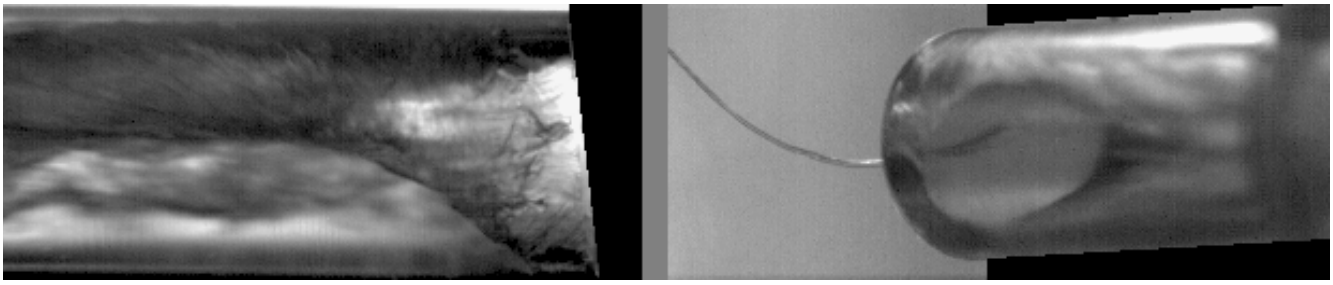

Figure 23: Representative image of film stage cavitation at CN=3 and full valve lift.

CONCLUSIONS

The transparent large-scale nozzle test rig proved to be extremely helpful in understanding the internal nozzle flow patterns, the dynamic behaviour of cavitation, its various forms and their development in gasoline multi-hole injectors especially through high-speed flow visualisation. A summary of the main findings is given below:

1. The internal nozzle flow in multi-hole injectors was found to be highly complex, transient and unstable. The visualisation results revealed that the flow into the nozzle holes originated either directly from the incoming annular flow above the six injection holes through a steep turning angle or from the deflected annular flow in-between two adjacent injection holes where the flow experienced a pressure gradient in the region between the two injection holes. This seemed to be the cause for the formation of vortices in the sac volume between the needle face and the two adjacent injection holes which, in turn, contributed to the formation of hole interconnecting strings.

2. The onset of cavitation was investigated for various flow rates, cavitation numbers and needle lifts. Contrary to expectations, the results showed that needle strings appeared first in the multi-hole gasoline injector prior to any cavitation hole structures. Needle string cavitation was initiated on the needle face and its formation has been attributed to a strong vortical flow around the hole axis. Once a needle string was created, it was then extended well inside the injection hole. The frequency of appearance of needle strings has increased with decreasing needle lift. In addition, low needle lifts resulted in more stable needle string structures.

3. At higher cavitation numbers, around 0.7 to 0.9, the first sign of geometric cavitation appeared at the top entrance of the hole while needle strings were still visible. Incipient geometric cavitation structures were very unstable and significantly affected by needle strings. Geometric cavitation in the hole inlet could occupy almost half of its perimeter by forming a canopy-shaped vapour pocket; unfortunately, these cavitation structures were found to be highly unstable.

4. The first evidence of well developed cavitation structures appeared at cavitation numbers greater than 1 when needle strings started to disappear. At that time, bubble clouds representing geometric cavitation started becoming more opaque and bubble coalescence more evident, which led to the formation of larger voids and ultimately localised vapour films.

5. Following the disappearance of the needle strings, another type of string known as ‘vortex string’ was captured during its development inside the injection hole. The formation mechanism for this was similar to that of the needle string and is linked to the presence of a strong vortex around the hole axis that was enhanced by the dense bubble vapour clouds present in the hole inlet; this effectively reduced the hole flow area and increased the local flow velocities.

6. Vortex string cavitation was found transiently to move upstream towards the hole inlet which triggered a bubble creation mechanism at the core of the vortex existing between two adjacent holes. The latter was the result of the interaction between the high momentum annular flow and the cross flow formed between two neighbouring injection holes. Once the bubbles were created at the core of that vortex, they could move towards the neighbouring hole forming interconnecting strings.

7. At cavitation numbers greater than 2, the pre-film stage cavitation structures were gradually replaced by film cavitation, associated with flow separation from the hole boundaries. Although there was a highly transient behaviour between pre-film and film cavitation structures, the latter did not show any correlation to the flow Reynolds number. Instead, the transition from bubbly cavitation films to fully separated two-phase flow showed to be a function of the needle lift. Further increase in the cavitation number (CN≥2.5) consolidated the establishment of a two-phase flow and clearly identifiable film stage cavitation structures.

8. It was found that the development of geometric cavitation was independent of the flow rate (Reynolds number), contrary to needle lift which appeared to dictate the formation of well-established gaseous pockets around the hole entrance. Low needle lifts were associated with higher velocities and more turbulent flow and resulted in bubblier (diffused) cavitation structures; higher lifts, on the other hand, enhanced the stability of these strings.

ACKNOWLEDGEMENT

The financial support provided by the Yamaha Motor Co. Ltd. and EPSRC (Grant GR/R71740/01) is gratefully acknowledged. The authors would also like to thank Mr Tom Fleming for his valuable technical support during the course of this work.

REFERENCES

1. Wirth, M., D. Zimmermann, R. Friedfeldt, J. Caine, A. Schamel, M. Davies, G. Peirce, A. Storch, K. Ries-Müller, K.P. Gansert, G. Pilgram, R. Ortmann, G. Würfel, J. Gerhardt, *A Cost Optimised Gasoline Spray Guided Direct Injection System for Improved Fuel Economy,* IMechE Seminar on Fuel

Economy and Engine Downsizing, 13 May, 2004, London.
2. Birth, I.G., M. Rechs, U. Spicher, and S. Bernhardt, *Experimental Investigation of the In-Nozzle Flow of Valve Covered Orifice Nozzle for Gasoline Direct Injection Engines.* 7th Int. Symp. Internal Combustion Diagnostics. 2006, pp. 59-78, Kurhaus Baden-Baden.
3. Roth, H., M. Gavaises, and C. Arcoumanis, *Cavitation Initiation, its Development and Link with Flow Turbulence in Diesel Injector Nozzles.* SAE Paper 2002-01-0214, 2002.
4. He, L. and F. Ruiz, *Effect of Cavitation on Flow and Turbulence in Plain Orifice for High-Speed Atomization.* Atomization and Sprays, 1995. **5**(6):pp. 569-584.
5. Soteriou, C., R.J. Andrews, N. Torres, M. Smith, and R. Kunkulagunta. *Through the Diesel Nozzle Hole - A Journey of Discovery II*. in Proc. ILASS-Europe, September 2-6, 2001 Zurich.
6. Arcoumanis, C., J.M. Nouri and R.J. Andrews, *Application of Refractive Index Matching to Diesel Nozzle Internal Flow. In* Proc. IMechE Seminar on Diesel Fuel Injection, April 14-15, 1992, London.
7. Arcoumanis, C., M. Gavaises, J.M. Nouri, E. Abdul-Wahab and R.W. Horrocks, *Analysis of the Flow in the Nozzle of a Vertical Multi Hole Diesel Engine Injector.* SAE Paper 980811, 1998.
8. Schmidt, D.P., C.J. Rutland and M.L.Corradini, *Cavitation in Two-Dimensional Asymmetric Nozzles*, SAE Paper 1999-01-0518, 1999.
9. Afzal, H., C. Arcoumanis, M. Gavaises, and N. Kampanis, *Internal Flow in Diesel Injector Nozzles: Modelling and Experiments.* IMechE Paper S492/S2/99, 1999.
10. Allen, J., G. Hargrave and Y. Khoo, *In-Nozzle and Spray Diagnostic Techniques for Real Sized Pressure Swirl and Plain Orifice Gasoline Direct Injectors,* SAE Paper 2003-01-3151, 2003.
11. Giannadakis, E., M. Gavaises, H. Roth, and C. Arcoumanis. *Cavitation Modelling in Single-Hole Diesel Injector Based on Eulerian-Lagrangian Approach*. Proc. THIESEL International Conference on Thermo- and Fluid Dynamic Processes in Diesel Engines, Valencia, 2004.
12. M. Gavaises and A. Andriotis, *Vortex Cavitation Inside Multi-hole Injectors for Large Diesel Engines and its Effect on the Near-nozzle Spray Structure*, SAE-Paper 2006-01-3151, 2006.
13. Mitroglou N, *Multihole Injectors for Direct-Injection Gasoline Engines,* PhD Thesis, The City University, London, 2006.
14. Gavaises, M., E. Abo-Serie and C. Arcoumanis, *Nozzle Hole Film Formation and its Link to Spray Characterization in Swirl-Pressure Atomizers for Direct Injection Gasoline Engines,* SAE Paper 2002-01-1136, 2002.
15. Allen, J., G. Hargrave, and Y. Khoo, *In-Nozzle and Spray Diagnostic Techniques for Real Sized Pressure Swirl and Plain Orifice Gasoline Direct Injectors*, SAE Paper 2003-01-3151, 2003.
16. Matsumura, E., T. Takashi, T. Takeda, S. Furuno and J. Senda, *Analysis of Visualized Fuel flow inside the Slit Nozzle of Direct Injection SI Gasoline Engine*, SAE Paper 2003-01-0060, 2003.
17. Roth, H., *Experimental and Computational Investigation of Cavitation in Diesel Injector Nozzle,* PhD Thesis, Imperial College London, 2004.